The Kinematics of Fountain Flow in Mold-Filling

Moldability criteria and process optimization for both reactive and thermoplastic injection molding hinge on the mold-filling step. The fluid mechanics of the filling step is typically described in terms of a one-dimensional main flow and a complex two-dimensional flow near the advancing front, often termed the "fountain flow." A unique apparatus which permits direct observation of the fountain flow in a rectangular cavity is described. The motion of tracer lines as well as the pathlines have been photographed for both Newtonian and shear-thinning liquids. The data show clearly the main flow, the transition to the front flow, and the deceleration and acceleration zones in the fountain flow, which lead to a "mushrooming" of the tracer line.

In addition, Galerkin finite-element analysis is used to predict the isothermal free-surface flow of a Newtonian liquid near the advancing front between parallel plates. The most interesting visualization of the calculated flow is obtained by tracking lines of material, thus producing numerical tracer experiments. The calculations show the widely varying residence times and the complex shear and extensional deformation histories of fluid elements as they move through the fountain flow region. The calculations are in agreement with the experiments and clarify previous results, both theoretical and experimental, that did not capture the details of the entire flow field.

D. J. Coyle
Polymer Physics and Engineering Branch
General Electric Company
Corporate Research and Development
Schenectady, New York 12301

J. W. Blake, C. W. Macosko
Department of Chemical Engineering
and Materials Science
University of Minnesota
Minneapolis, MN 55455

Introduction

The flow immediately behind an advancing interface when one fluid displaces another from a narrow channel is commonly known as fountain flow (Rose, 1961). Fluid entering the front region decelerates in the direction of flow and acquires a transverse velocity, spilling outward toward the wall. This type of flow is important in coating operations, oil recovery, and polymer processing.

In thermoplastic injection molding, material deformation and orientation that takes place during the filling stage has a major effect on the morphology and ultimate properties of an injection molded part. The bulk of the flow field in mold-filling is accurately described as a one-dimensional shear flow, but it is the two-dimensional free-surface flow close to the advancing melt front that is responsible for much of the molecular orientation.

In reactive injection molding, one must have detailed knowledge of the resident time distribution in order to find the temperature and conversion distributions throughout the mold. The front flow is thus in a sense even more important here than in thermoplastic injection molding. In either case, accurate analysis of the fountain flow must be incorporated in developing complete mold-filling models used to evaluate injection molding processes.

With interests in interfacial flow during immiscible fluid displacement, several researchers observed fountain flow streamlines in capillaries (Brown et al., 1980; Dussan, 1977; Bhattarchargi and Savic, 1965). While these results are significant, they do not observe tracer line motion through the front flow. Furthermore, in these cases the displaced fluid is a liquid, not air, as in typical polymer processing cases.

Researchers interested in thermoplastic injection molding have also observed the fountain flow experimentally in the past, but have not visualized the detailed kinematics of the flow. In tracer studies (Spencer and Gilmore, 1951; Gilmore and Spencer, 1951) a spreading radial flow in a disk-shaped cavity was used, where the tracer particle motion was observed through the

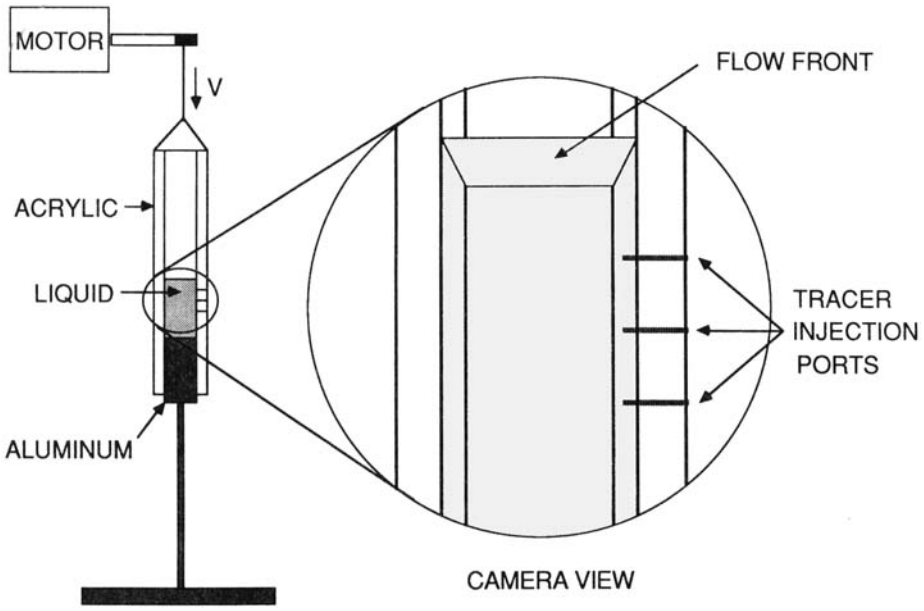

Figure 1. Fountain flow visualization apparatus.
Viewing angle is from below

broad flat top portion of a mold. Polymeric tracer particles were seen overtaking the slower moving front and being deposited at the cold mold wall. Later experiments by Schmidt (1974, 1978) yielded more detailed observations of the fountain flow during filling. Fine details of the flow were surmised from the location of tracer particles in cross sections of the final part. In both cases, only the cumulative effects of the fountain flow were seen. To elucidate the detailed kinematics of the flow, it is necessary to observe the flow through the narrow slit between the two mold halves during the entire filling process.

There have been a number of approximate models of fountain flow, such as those of Bhattachargi and Savic (1965), Tadmor (1974), and Kafka and Dussan (1979). In addition, a number of workers have incorporated such models in mold-filling analyses, including White and Dietz (1979), Domine and Gogos (1980), Castro (1980), Castro and Macosko (1982), Manzione (1981), Kamal et al. (1982, 1985), and Manas-Zloczower et al. (1986). Huang (1978) attempted a detailed numerical solution using the marker-and-cell method, but his formulation violates symmetry near the interface. Silliman (1979), Lowndes (1980), and Mavridis et al. (1986a) have used the finite-element method to accurately calculate the flow field, but none of these has focused on the details of the deformation of material as it moves through the flow. Very recently Mavridis et al. (1986b) did focus on this problem, but as will be shown later captured only part of the deformation.

This work is an extensive examination of the kinematics of fountain flow. New experiments are reported that allow the visualization of the flow field and material line deformation in much greater detail than any previously reported. Furthermore, Galerkin finite-element analysis is used to predict the two-dimensional free surface flow at the front, from which material deformations can be calculated and compared with the experiments. The results provide a better understanding of fountain flow and aid in the interpretation of previous experimental results.

Table 1. Experimental Conditions and Dimensionless Groups

	Newtonian Experiments	Shear-thinning Experiments
V	0.002 m/s	0.06 m/s
ρ	970 kg/m^3	1,000 kg/m^3
μ	52.5 Pa · s	11.0 Pa · s
σ	0.021 N/m	0.075 N/m
Ca	5	8.8
St	33	5.4
Re	0.0007	0.103

Visualization of Fountain Flow

The experimental apparatus used to observe the fountain flow is shown in Figure 1. The key experimental improvement over the previously mentioned injection molding studies is that the flow is viewed through the narrow side rather than through the wide top, allowing the detailed kinematics of the flow to be seen. In addition, the setup allows one to view the mold-filling flow in a reference frame translating with the flow front simply by fixing the position of the camera and the bulk fluid and translating the walls of the apparatus. A constant-speed motor is used to lower a transparent acrylic mold over a stationary aluminum plug that rests on the floor. The test fluid is poured into the region above the aluminum with the acrylic mold in the position shown. The liquid seal between the acrylic and the aluminum is maintained by two O-rings. The inside dimensions of the mold are 0.038 x 0.114 x 1.016 m. When the motor is turned on, the downward motion of the acrylic over the aluminum plug creates three regions of flow: a fountain flow just behind the free surface, a plane shear main flow behind the fountain flow, and a recirculating flow near the aluminum plug. A sufficient amount of liquid is used so that the recirculating flow does not interfere with observations of the main flow and fountain flow.

To make visible the motion of a line of tracer material experiencing the fountain flow, the tracer is injected via a needle through ports in the side of the acrylic into the quiescent fluid. Care is taken to inject the tracer in the plane of symmetry between front and back walls in order to observe only the fountain flow due to the side walls. To begin the fountain flow, the motor is turned on and the ensuing tracer motion is recorded on videotape or film. Because the acrylic walls move during the experiment, the free surface position, and hence the camera position, does not move. In this frame of reference the net flow rate is zero. Liquid near the walls moves in the same direction as the walls (away from the flow front), while liquid in the center moves in the opposite direction (toward the flow front). The flow is the same as one would observe if a camera were moved at the same speed as the flow front while a mold was being filled. The camera view, as shown in Figure 1, looks up from underneath the interface. This is because in a straight-on view the interfacial curvature at the near wall would hide the tracer motion near the interface. The wall velocity, or equivalently, the front velocity, is determined by attaching a meter stick to the moving

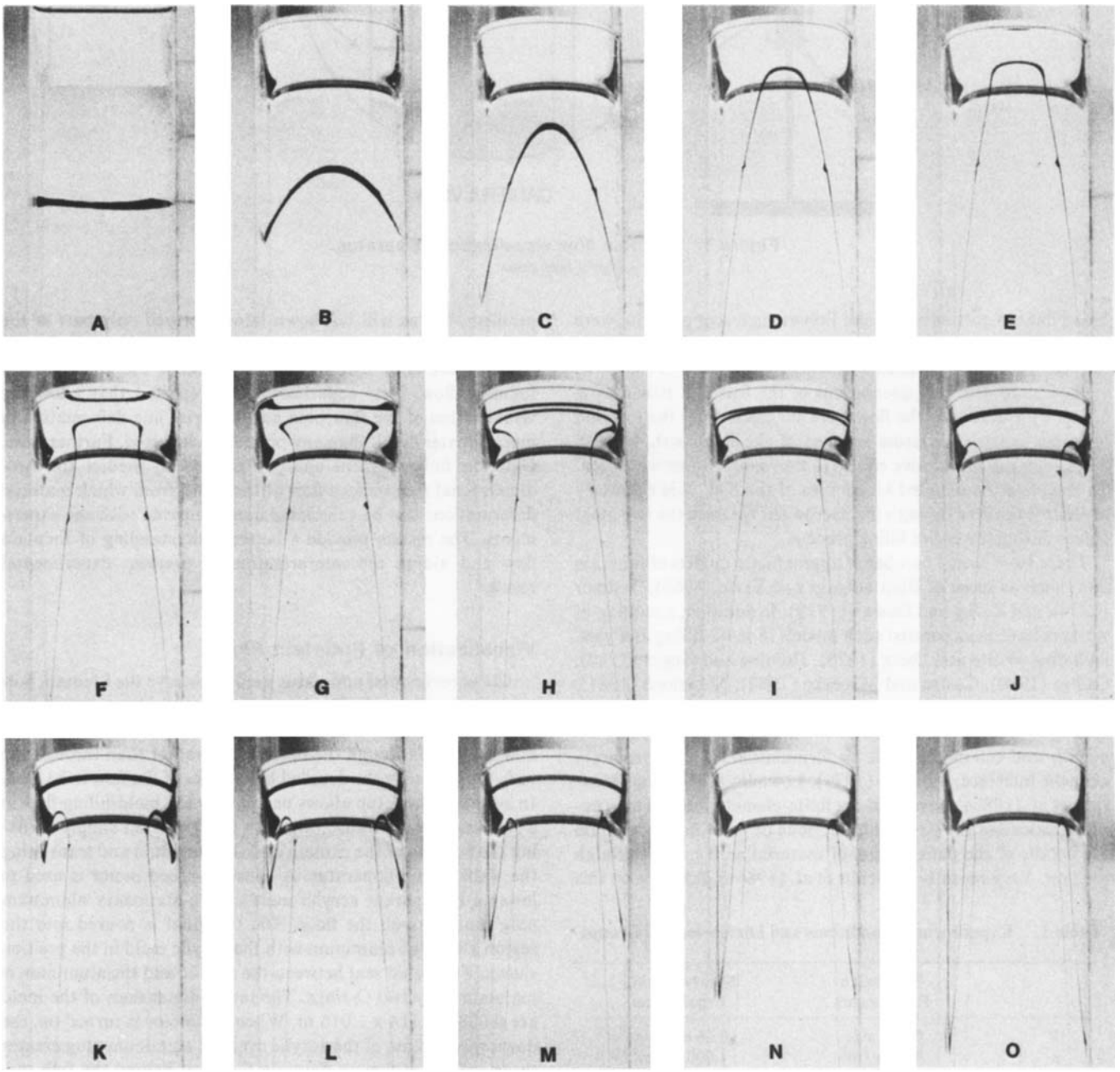

Figure 2. Deformation of tracer line in fountain flow of Newtonian silicone oil.
Reflection of dye first appears in meniscus in (e)
A = 0 *s*, *B* = 10 *s*, *C* = 20 *s*, *D* = 35 *s*, *E* = 40 *s*,
F = 45 *s*, *G* = 50 *s*, *H* = 55 *s*, *I* = 60 *s*, *J* = 65 *s*,
K = 70 *s*, *L* = 75 *s*, *M* = 85 *s*, *N* = 95 *s*, *O* = 105 *s*,

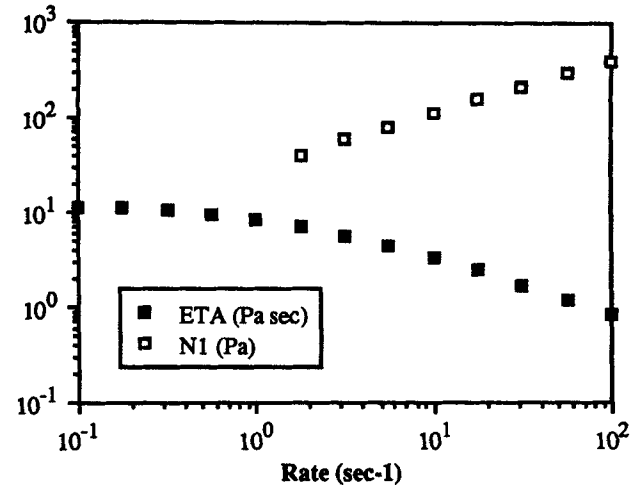

Figure 3. Steady shear viscosity and normal stress behavior of shear-thinning solution.
5% Rheothik in water

acrylic mold and recording the time during the run with a stopwatch. Tracer line motion is observed for both Newtonian and shear-thinning liquids. The experimental conditions and appropriate dimensionless numbers are given in Table 1, permitting quantitative comparison to the theoretical predictions.

Sequential photographs of tracer motion in a Newtonian fluid (Dow Corning 200 Fluid) are shown in Figure 2. Carbon black dispersed in the same silicone oil is the tracer material. The initial response of the tracer line, Figure 2a–c, reflects the plane Poiseuille main flow. Once material enters the fountain flow, it undergoes some extensional flow and acquires a transverse velocity component, giving rise to the mushroom shape in Figure 2g. Material spills outward toward the side wall, eventually being pulled along with the wall and reentering the main flow as shown in Figure 2h–o. Some amount of the tracer always remains at the interface, forming an ever-thinning filament connecting to the V-shaped region near the wall. As tracer material approaches the interface, its mirror image appears. This mirror image appears distorted when reflected off the curved surfaces of the underside of the interface. The meeting of the tracer curve with its mirror image is useful in defining the shape and position of the interface. Once the interface's position is known, the front thickness can be determined.

At first glance, these results may seem fundamentally different from those using polymer melts reported earlier. The analysis performed later will show that these results are merely a more detailed look at the same phenomena.

The effect of shear-thinning behavior is examined by repeating the tracer experiments using a 5 wt. % aqueous solution of Henkel Corporation's Rheothik 80-11, a transparent, water-soluble polysulfonic acid. The rheology of the solution, mea-

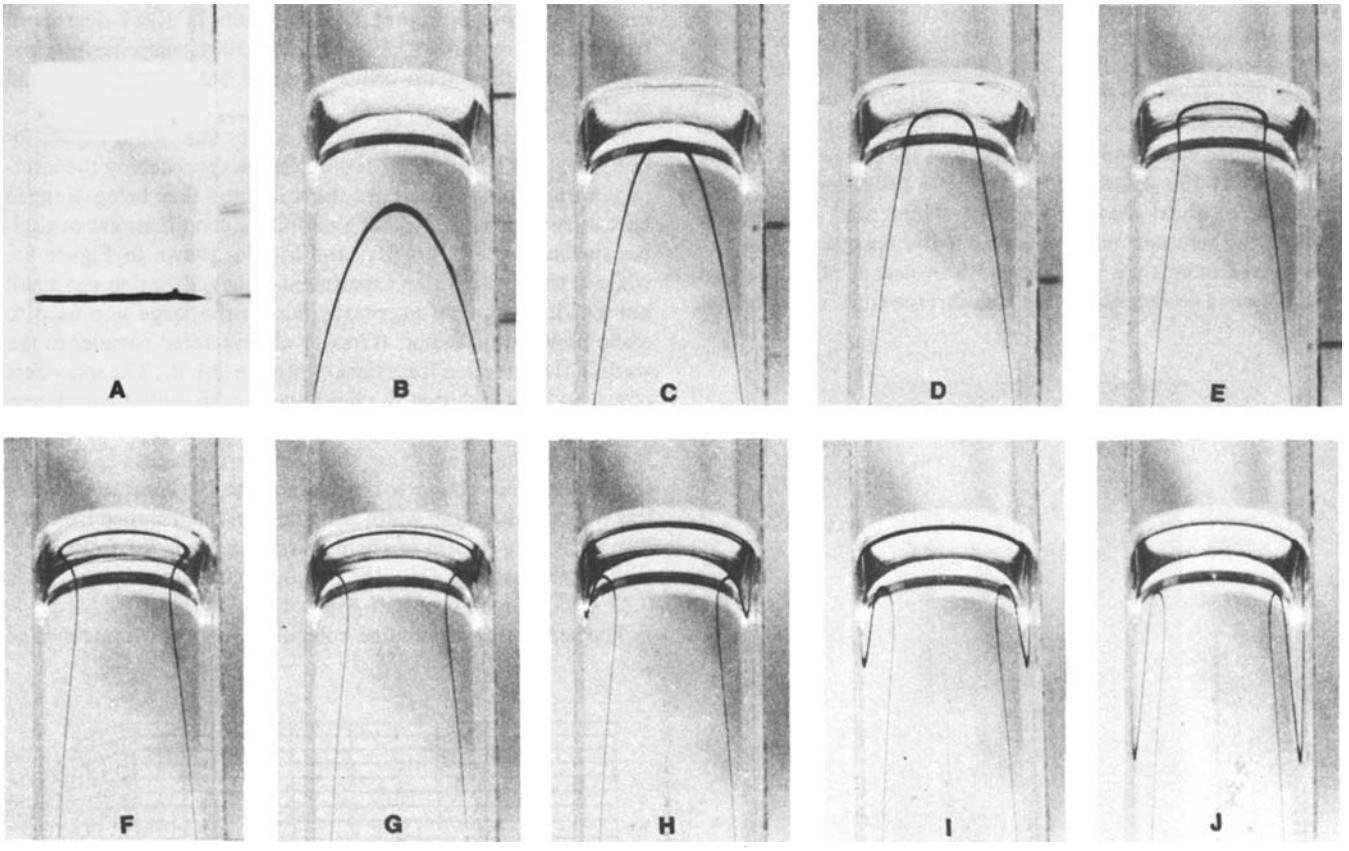

Figure 4. Deformation of tracer line in fountain flow of shear-thinning solution.
A – 0 *s*, *B* – 0.5 *s*, *C* – 1.0 *s*, *D* – 1.25 *s*, *E* – 1.5 *s*,
F – 1.75 *s*, *G* – 2.0 *s*, *H* – 2.25 *s*, *I* – 2.5 *s*, *J* – 3.0 *s*,

sured on a Rheometrics System IV rheometer, is shown in Figure 3. Blue food dye dispersed in Rheothik solution is the tracer material. The motor speed is set much higher for these experiments in order to obtain shear rates in the shear-thinning range; the wall shear rate in the main flow is $\sim 13\ s^{-1}$. Sequential photographs, taken at a rate of $\sim 4/s$, produce the results shown in Figure 4. In spite of the large differences in speed and liquid rheology, the tracer line deformation is almost identical to the Newtonian case. For either liquid, the thickness of the front region is less than one-half of the total gap thickness, being slightly thicker in the Rheothik case, probably due to smaller gravitational effects as will be shown later.

Streamlines are observed for both fluids by feeding the tracer material up through a tube that passes through the aluminum plug and then branches into seven separate tubes. The tracer is either preplaced in the quiescent test fluid or injected during the flow. The results for the shear-thinning solution are shown in Figure 5. Both the shape of the interface and the extensional flow in the vicinity of the stagnation are evident. These streamlines, viewed as a set of nested loops, show clearly the cumulative effect of the fountain flow as a transfer of fluid from forward-moving central streamlines of the main flow to backward-moving streamlines near the wall.

Computation of Fountain Flow

The *Galerkin finite-element method* is used to calculate the steady two-dimensional free surface flow for an incompressible Newtonian liquid under isothermal conditions. The flow domain is defined in Figure 6, while the Navier-Stokes equations need only be solved over half this domain because of symmetry. Both inertia and gravity terms are included, although the former was never significant. Boundary conditions of no slip at the wall and no transverse velocity nor shear stress at the symmetry line are imposed. At the upstream boundary, a fully developed one-dimensional shear flow is imposed. Numerical experiments showed the solutions to be accurate if the upstream boundary was placed more than one gap-width upstream of the contact line. There is no flux across the free surface (it is a streamline)

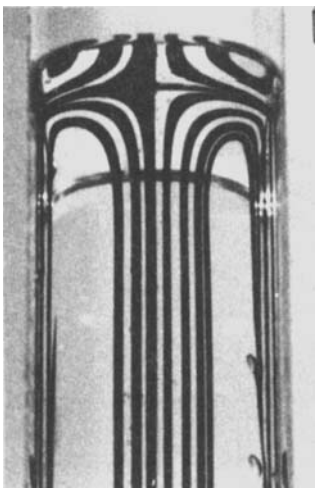

Figure 5. Streamlines in fountain flow of shear-thinning solution.

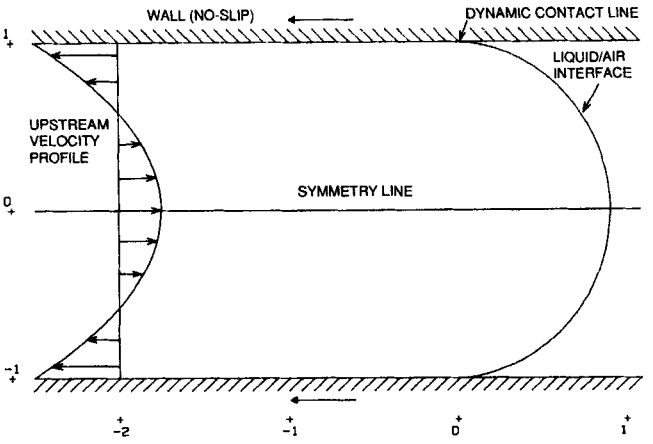

Figure 6. Definition of fountain flow.

where the traction is given by the capillary pressure (surface tensional times curvature) along with vanishing shear stress. A 180° contact angle was assumed where the free surface meets the solid wall, which alleviates the need for a slip boundary condition.

The nonlinear equation system is solved by the Galerkin finite-element method as described by Kistler and Scriven (1983) and Coyle et al. (1986). The velocities, pressure, and free surface location are solved for simultaneously by a full Newton iteration. A typical fine mesh of 127 biquadratic isoparametric rectangles is shown in Figure 7. This results in 1,281 degrees of freedom and requires 75 s on an IBM 3081 computer for four Newton iterations with convergence of both the updates and residuals to 10^{-8}.

Streamlines, shown in Figure 8, are as one would expect for this flow, with liquid in the central region approaching the interface, turning outward toward the walls, and then being dragged back with the walls. Typical mold-filling conditions are negligible surface tension, gravity, and inertia, shown in Figure 8a, while in the visualization experiments, surface tension was small but gravity was very important due to the large gap used to make observation easier. (Gravity always acted parallel to the walls in the direction from the air into the liquid.) The sole effect of gravity was to flatten the interface considerably (except very near the walls) and thus shrink the two-dimensional flow region. It is interesting to note that the upstream influence of the flow front, measured relative to the contact line, is a constant value of less than one half-gap width. In addition, the distance from the contact line to the tip of the meniscus is predicted to be 0.28, while that measured from the photographs of the experiment is 0.27 ± 0.03 (in units of half-gap width).

The separating streamline coincides with the symmetry line

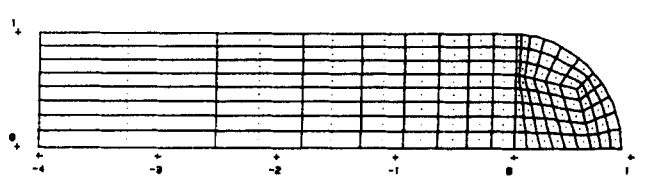

Figure 7. Finite-element discretization of one half of symmetric flow domain.

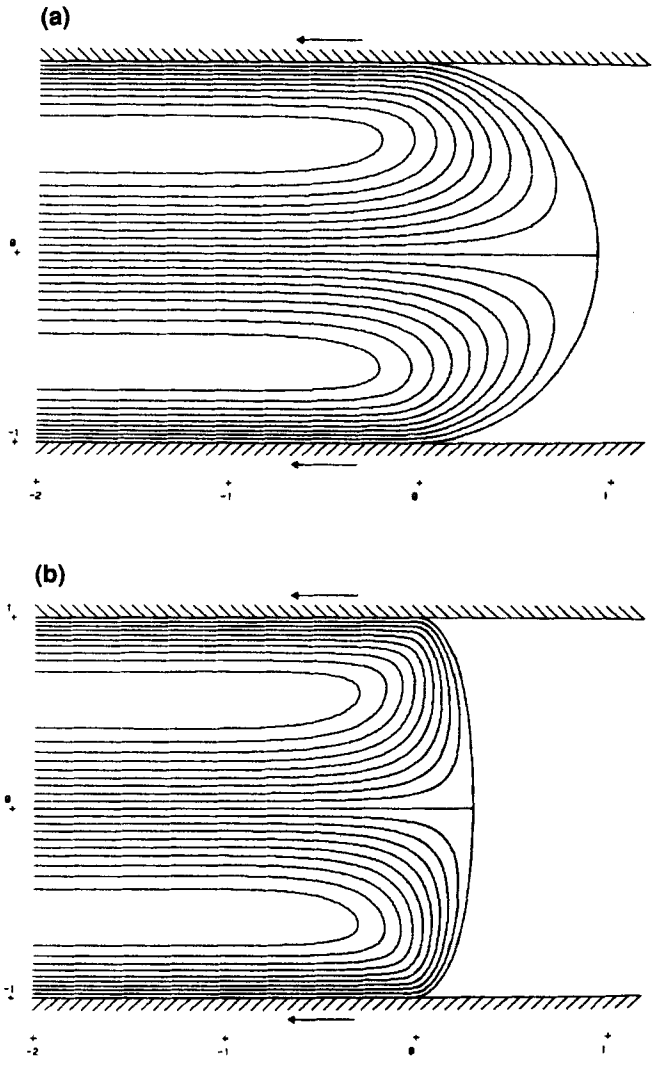

Figure 8. Calculated streamlines for fountain flow.
a. Typical mold-filling conditions, $Ca = \infty$, $St = 0$
b. Parameters of Newtonian experiments where gravity was important, $Ca = 5.0$, $St = 33$

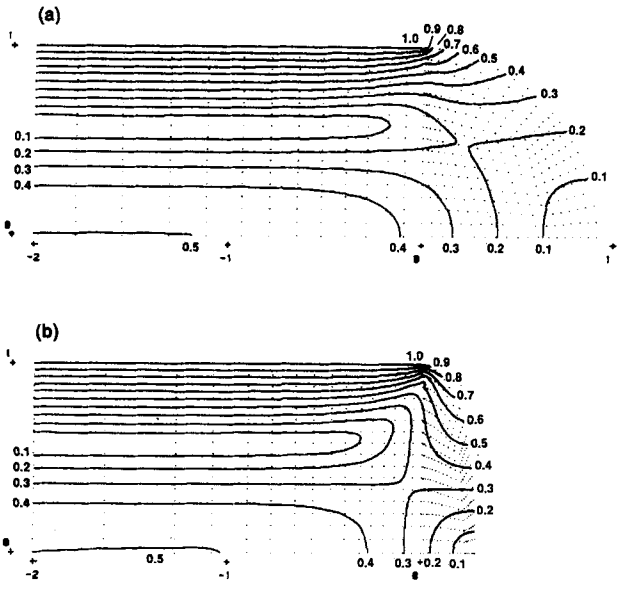

Figure 9. Calculated liquid speed showing stagnation regions at center of the one-dimensional flow region and at tip of liquid/air interface (symmetric half only).
a. $Ca = \infty$, $St = 0$; b. $Ca = 5.0$, $St = 33$

and terminates at a stagnation point on the free surface. This stagnation region, the two-dimensional flow around it, and the one-dimensional upstream flow, are the keys to understanding how a material line (tracer line of the previous experiment) deforms as it passes through the fountain flow. This becomes clear when one considers the speed of the liquid, shown in Figure 9, alongside the streamlines. Any tracer near the symmetry line decelerates as it approaches the interface and takes a long time to pass through this region. In addition, any tracer that is near the central (with respect to the half-gap) stagnant region of the one-dimensional flow will also take a long time to pass through the front. Thus, as the line approaches the front, tracer near this central region and symmetry region is held back, while that in between moves faster and spills outward toward the walls to form a V pattern near the wall.

The tracer experiment can be simulated by numerically tracking a large number of points (~350) through the calculated velocity field. Figure 10 shows the tracer line deformation for typical mold-filling conditions, while Figure 11 shows that corresponding to the experimental conditions. Both cases show the mushrooming of the tracer line as it passes through the fountain flow. Initially, in the one-dimensional shear flow, the line deforms into a parabolic shape, the tip of which approaches the interface. On encountering the flow front, the tip decelerates and is stretched toward the walls, with material on either side moving faster to form protrusions. Near the walls these protrusions, which are themselves V-shaped, are swept back parallel to the walls, forming an ever more extended mushroom shape. The sole difference between the two flow conditions is that gravity shortens the length scale of the fountain flow region, thus making the material line deformation more abrupt and allowing the tracer to get closer to the free surface and walls in a shorter period of time. It should be noted that the predicted tracer lines

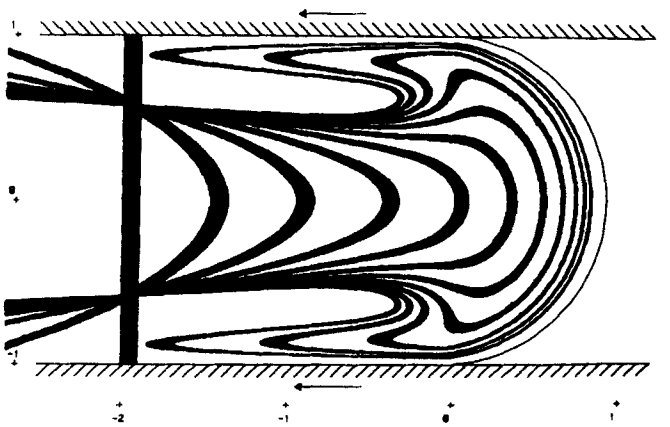

Figure 10. Calculated tracer line deformation as a function of time at typical mold-filling conditions.
$\Delta t = 1.0$, $Ca = \infty$, $St = 0$

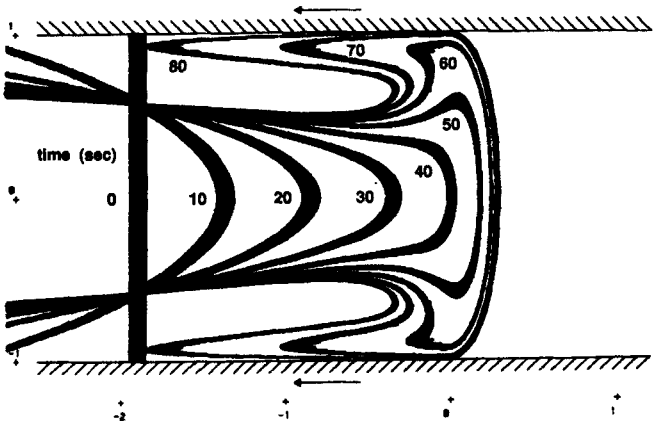

Figure 11. Calculated tracer line deformation as a function of time at the conditions of Newtonian experiment of Figure 2.

$Ca = 5.0, St = 33$

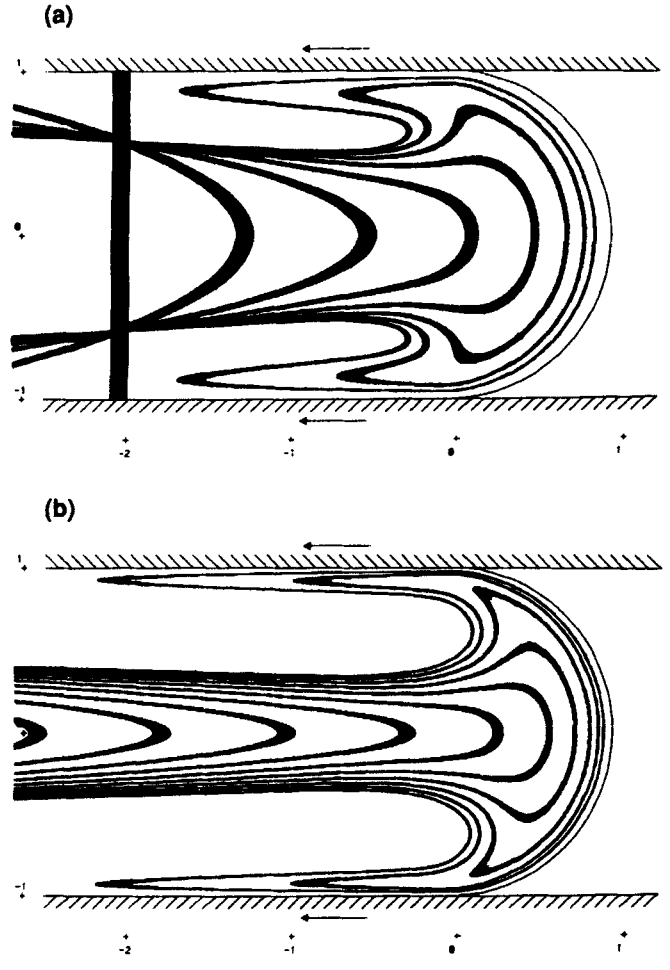

Figure 12. Effect of initial position x_o of tracer line on its deformation with time.

$\Delta t = 1.5$

a. $x_o = -2$; b. $x_o = -10$

of Figure 11 are virtually indistinguishable from the photographs of Figure 2, both in terms of their location and their relative thickness. Figure 12 illustrates the effect of a tracer spending more time deforming in the shear flow before encountering the flow front. In doing so, the line deforms into a sharper, more pointed, bulletlike shape before it mushrooms and forms sharper V patterns that are closer to the wall. In either case, the largest amount of tracer winds up in the vicinity of the V.

One of the most prominent effects of fountain flow in mold-filling is that material first to enter the mold travels the shortest distance downstream of the entrance, when compared to all other material that has encountered the flow front. This effect is clearly visualized by examining three consecutive material lines as in Figure 13. The tracers enter the mold in the order 1, 2, 3, and subsequently are found near the wall in the reverse order. But as a direct consequence of the kinematics causing the mushrooming effect, some amount of the tracers near the symmetry plane should be found further down the mold and in particular they should be found in their original order at the far end of the mold when it has filled. The extreme extension the tracers experience as they move with the interface makes it unlikely that they would be visible at the end of a mold-filling experiment. Indeed, they do not appear in Schmidt's (1974) photographs. For example, in the experiment shown in Figure 2 the tracer at the interface is fading from view (Figure 2h) after the interface has traveled only five gap-widths with respect to the walls.

Thus, to fully understand the results of mold-filling tracer experiments one must consider the effect of the dilution of the dye due to stretching of the tracer line. This can be simulated in the following manner. The calculation of material line position is accomplished by tracking a large number of discrete points as they move through the flow. Defining a strain measure s as the distance between adjacent points at time t divided by their initial separation allows the relative stretching of the material line to be quantified. By setting a critical strain s^* such that only the points that have been separated by less than this strain are plotted, one can simulate approximately what happens in an actual experiment. This effect is illustrated in Figure 14. As the critical strain (which can be thought of as a measure of the initial dye concentration) is decreased, the material line appears to split in two when it approaches the interface, and what appears to be

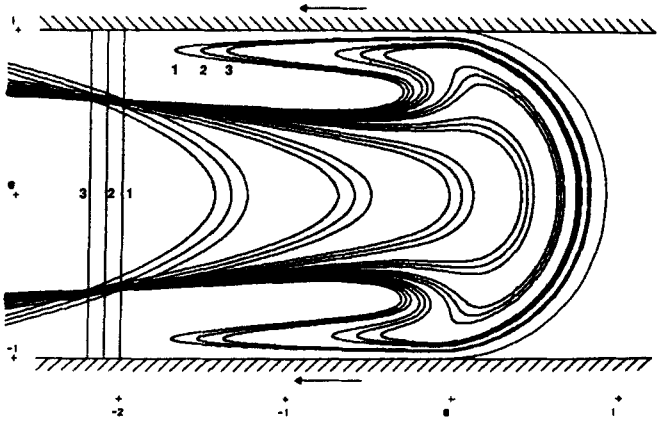

Figure 13. Deformation and rearrangement of three sequential tracer lines.

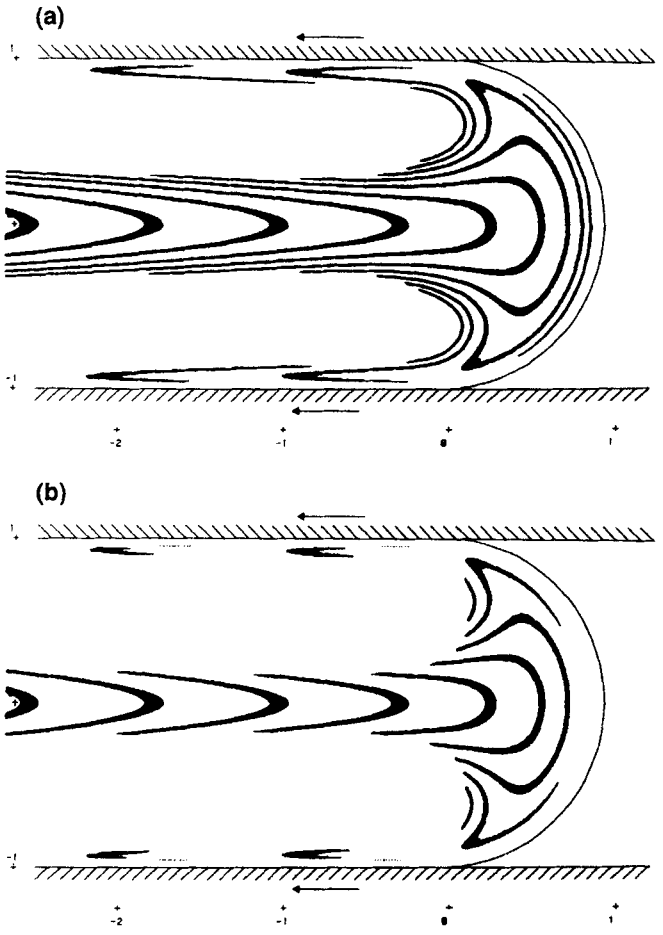

Figure 14. Simulated effect of tracer dilution due to stretching on observed tracer line deformation.

a. $s^* = 2{,}000\%$; b. $s^* = 1{,}000\%$

isolated V patterns are carried back by the walls. The same patterns are shown developing in a fixed frame of reference (stationary walls, moving interface) in Figure 15. The apparently isolated, reverse-order V patterns located along the walls are exactly what was observed in the mold-filling experiments of Schmidt (1974), but Figure 14a shows that these patterns are simply one piece of the material line global structure that must always be present. In fact, Figure 2n–o shows that in the current experiment the dye remains most highly visible near the tip of the V and fades from view elsewhere.

Recent work by Mavridis et al. (1986b) also involves numerical tracer experiments and is able to duplicate the patterns photographed by Schmidt, but shows the V's forming long after the material has passed through the fountain flow. This might at first seem to contradict the current results that show the V's forming during the mushrooming stage. But by tracking only a limited amount of material rather than tracking material spanning the entire gap, Mavridis et al. see only a small segment of the deformation. If they change the location of their initial material, they get a different view of the deformation. Their apparent evolution in time of a V is a consequence of the fact that the material which forms the V tip at one time is not the same as that forming the tip at a later time. This effect is clearly shown in Figure 16, indicating that Mavridis' results are consistent with the more general results presented here.

Another experimentally observed phenomenon to which fountain flow kinematics are relevant is that in nonisothermal thermoplastic mold-filling tracer experiments the tip of the V appears to lie at or near the boundary of the quenched layer of polymer found at the walls (Schmidt, 1981). A plausible explanation is shown qualitatively in Figure 17. The V shape is formed in the fountain flow, but only a segment of that closest to the wall is solidified, leaving the tip of the V initially outside this quenched layer. The material in the flow continues to deform in steady shear, thus causing the tip of the V to migrate to the interface. While the precise length scales are actually deter-

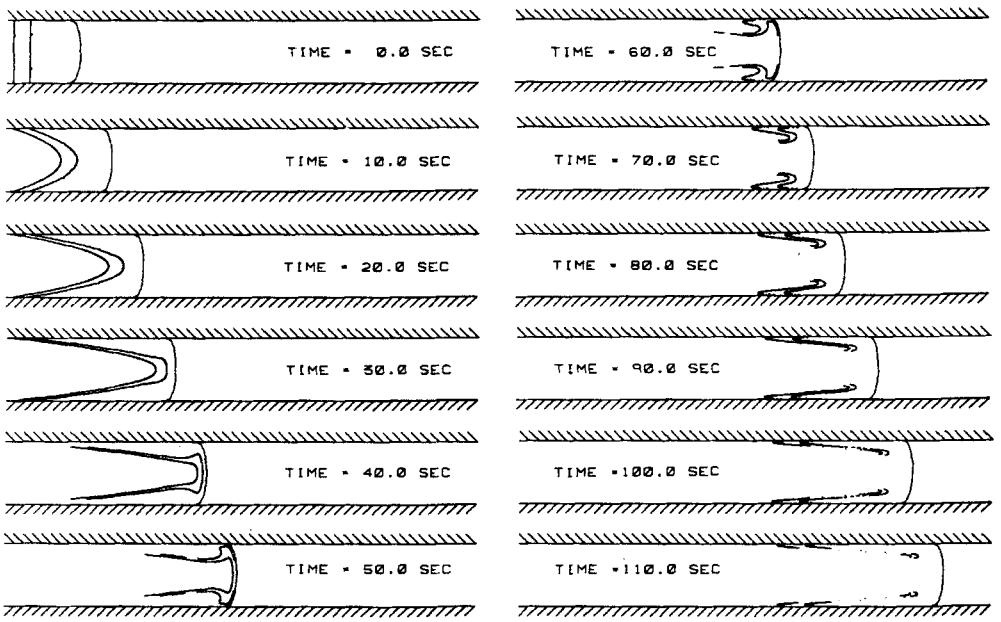

Figure 15. Evolution of two tracer lines in a frame of reference where the mold walls are stationary.

$Ca = 5$, $St = 35$, $s^* = 1{,}000\%$

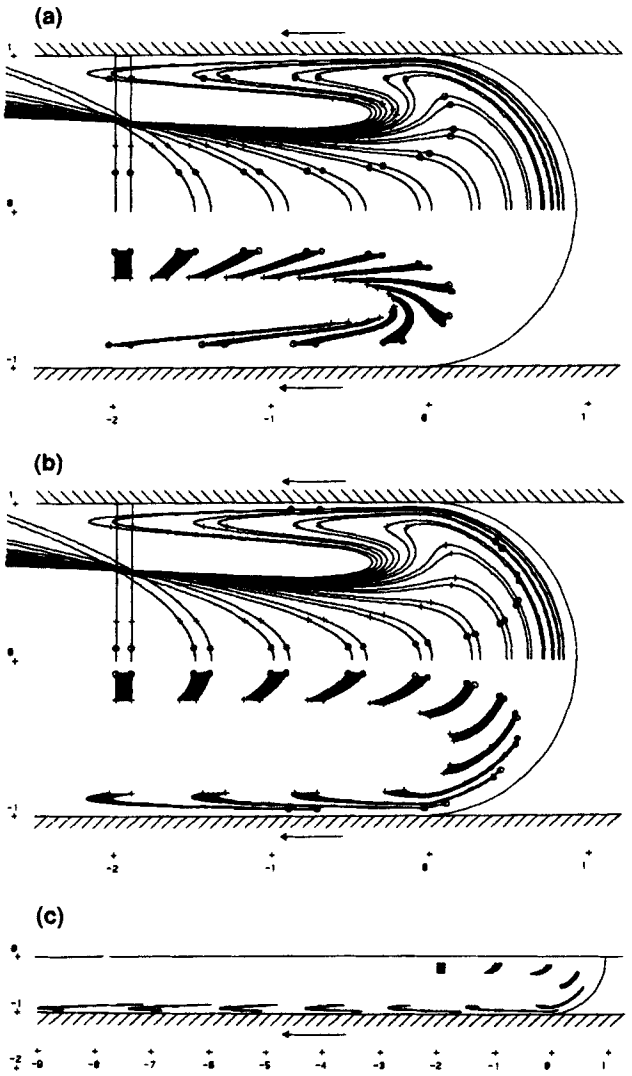

Figure 16. Sensitivity of tracer patterns to initial tracer location.

Lower half of each figure shows only that material between + and the *o*

Upper half of each figure shows an entire strip of material from symmetry line to wall

Note scale change in (c), which for clarity only shows the lower half

mined by the nonisothermal flow with solidification, the global structure shown here is probably a good approximation.

One last phenomenon into which this work gives insight is the orientation distribution in injection-molded thermoplastic parts. The kinematics of the fountain flow, as visualized by tracer line deformation, clearly shows that the high orientation at the surface arises from the extensional flow near the intersection of the free surface and the symmetry plane. The calculated extension rate here is 0.4 V/L for infinite capillary number; see Figure 9. Just inside this region is material that encountered a much weaker mixed flow (shear plus extension) as it traveled through the fountain region. Next to this is the material that is more highly oriented due to the shear flow far from the melt front, while at the core most of the orientation relaxes before solidification. It is the structure near the wall that is governed solely by the fountain flow.

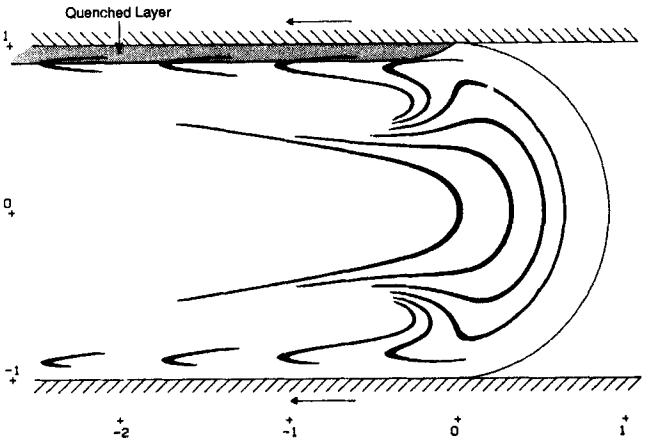

Figure 17. Simulated effect of solidification at wall on observed tracer patterns.

$Ca = \infty$, $St = 0$, $s^* = 700\%$

Conclusions

The combination of experiment and theory presented here leads to a detailed description of the kinematics of fountain flow in mold-filling. The unique experimental apparatus allows a visualization of the flow that is far more complete than those reported previously. The mushrooming of a tracer line as it experiences the fountain flow is clearly shown, as is the formation of V patterns in the vicinity of the walls.

Finite-element solutions of the Navier-Stokes equations give the detailed flow field, from which material line deformations are calculated. The results were in complete agreement with the experiments. Computation of the relative stretching of the material line allows simulation of the effect of dilution of the dyes in the experiments. These simulations, backed up by experimental observations of tracer visibility, show that the tracer experiments of Schmidt (1974) are consistent with the current results, but the earlier experiments show only a fraction of a larger, more complete picture. Similarly, recent calculations of Mavridis et al. (1986b) use limited conditions and thus also represent a subset of the results shown here.

The fact that Newtonian isothermal considerations alone can predict many phenomena in thermoplastic injection molding associated with fountain flow is perhaps at first surprising. But in fact this flow is largely determined by conservation of mass together with the boundary conditions, with only the details of the length scales being influenced by conservation of momentum. The experiments show that shear-thinning is relatively unimportant, while nonisothermal effects should not alter the overall kinematics significantly. By the same arguments, viscoelasticity probably has little effect on the overall kinematics of fountain flow (other than changing the length scales), but planned experiments should settle this issue conclusively.

Acknowledgment

The authors wish to thank Jayesh Bellare of the University of Minnesota for providing photographic equipment and many helpful suggestions for the visualization experiments. The experimental work was supported by the National Science Foundation (NSF/CBT-8512120) and the Owens-Corning Fiberglass Corporation.

Notation

Ca = capillary number, $\mu V/\sigma$, viscous/surface tension force ratio
g = gravitational constant
L = half-gap length
Re = Reynolds number, $\rho VL/\mu$, inertial/viscous force ratio
St = Stokes number, $\rho gL^2/\mu V$, gravity/viscous force ratio
s^* = critical strain at which adjacent points are not plotted
t = dimensionless time, units of L/V
V = average injection velocity
x_o = initial upstream distance (units of L) of tracer line

Greek letters

μ = viscosity
ρ = density
σ = surface tension

Literature cited

Bhattacharji, S., and P. Savic, "Real and Apparent Non-Newtonian Behavior in Viscous Pipe Flow of Suspensions Driven by a Fluid Piston," *Proc. 1965 Heat Trans. Fluid Mech. Inst.*, 248 (1965).

Brown, C. E., T. J. Jones, and E. L. Neustadter, "Interfacial Flow During Immiscible Displacement," *J. Colloid Interf. Sci.*, **76**, 582 (1980).

Castro, J. M., "Mold Filling and Curing Studies for the Polyurethane RIM Process," Ph.D. Thesis, Univ. Minnesota (1980).

Castro, J. M., and C. W. Macosko, "Studies of Mold Filling and Curing in the Reaction Injection Molding Process," *AIChE J.*, **28**, 250 (1982).

Coyle, D. J., C. W. Macosko, and L. E. Scriven, "Film-splitting Flows in Forward Roll Coating," *J. Fluid Mech.*, **171**, 183 (1986).

Domine, J. D., and C. G. Gogos, "Simulation of Reactive Injection Molding," *Polym. Eng. Sci.*, **20**, 847 (1980).

Dussan V, E. B., "Immiscible Liquid Displacement in a Capillary Tube: The Moving Contact Line," *AIChE J.*, **23**, 131 (1977).

Gilmore, G. D., and R. S. Spencer, "Photographic Study of the Polymer Cycle in Injection Molding," *Mod. Plastics*, **28**, 117 (1951).

Huang, C. F., "Simulation of the Cavity Filling Process with the Marker-and-Cell Method in Injection Molding," Ph.D. Thesis, Stevens Inst. Technol. (1978).

Kafka, F. Y., and E. B. Dussan V, "On the Interpretation of Dynamic Contact Angles in Capillaries," *J. Fluid Mech.*, **95**, 539 (1979).

Kamal, M. R., E. Chu, P. G. Lafleur, and M. E. Ryan, "Computer Simulation of Injection Mold Filling for Viscoelastic Melts with Fountain Flow," *Soc. Plast. Eng. Ann. Tech. Conf.*, Washington, DC, 818 (1985).

Kamal, M. R., and P. G. Lafleur, "Computer Simulation of Injection Molding," *Polym. Eng. Sci.*, **22**, 1066 (1982).

Kistler, S. F., and L. E. Scriven, "Coating Flows," *Computational Analysis of Polymer Processing*, J. R. A. Pearson and S. M. Richardson, eds., Applied Science Pub., London, New York, p. 243.

Lowndes, J., "The Numerical Simulation of the Steady Movement of a Fluid Meniscus in a Capillary Tube," *J. Fluid Mech.*, **101**, 631 (1980).

Manas-Zloczower, I., J. W. Blake, and C. W. Macosko, "Space-Time Distribution in Filling a Mold," *Polym. Eng. Sci.*, to appear in a special issue on Reactive Processing (1987).

Manzione, L. T., "Simulation of Cavity Filling and Curing in Reaction Injection Molding," *Polym. Eng. Sci.*, **21**, 1234 (1981).

Mavridis, H., A. N. Hrymak, and J. Vlachopoulos, "Finite-element Simulation of Fountain Flow in Injection Molding," *Polym. Eng. Sci.*, **26**, 449 (1986a).

———, "Deformation and Orientation of Fluid Elements Behind an Advancing Flow Front," *J. Rheol.*, **30**, 555 (1986b).

Rose, W., "Fluid-Fluid Interfaces in Steady Motion," *Nature*, **191**, 242 (1961).

Schmidt, L. R., "A Special Mold and Tracer Technique for Studying Shear and Extensional Flows in a Mold Cavity During Injection Molding," *Polym. Eng. Sci.*, **14**, 797 (1974).

———, "Velocity Field Rearrangement in Stagnation Flow Leading to Diverging Radial Flow Between Parallel Plates," *J. Rheol.*, **22**, 571 (1978).

———, "The Interrelationship of Flow, Structure, and Properties in Injection Molding," *Proc. 2nd World Cong. Chem. Eng.*, **6**, 516 (1981).

Silliman, W. J., "Viscous Film Flows with Contact Lines," Ph.D. Thesis, Univ. of Minnesota (1979).

Spencer, R. S., and G. D. Gilmore, "Some Flow Phenomena in the Injection Molding of Polystyrene," *J. Colloid Sci.*, **6**, 118 (1951).

Tadmor, Z., "Molecular Orientation in Injection Molding," *J. Appl. Polym. Sci.*, **18**, 1753 (1974).

White J. L., and W. Dietz, "Some Relationships Between Injection Molding Conditions and the Characteristics of Vitrified Molded Parts," *Polym. Eng. Sci.*, **19**, 1081 (1979).

Manuscript received May 15, 1986, and revision received Jan. 6, 1987.